Nonlinear Simulation and Characterization of Devices with HTS Transmission Lines Using Harmonic Balance Algorithms

Carlos Collado, Jordi Mateu, Juan M O'Callaghan

Abstract — This work presents the use of Harmonic Balance to simulate the nonlinear behavior of HTS transmission lines. Good agreement with theoretical cross-checks is found. We also show the use of this algorithm to fit the model of HTS lines from experimental measurements. We illustrate this by fitting several types of experimental data, and discuss how to avoid ambiguity in this fitting.

Index Terms— Filters, Harmonic Balance, nonlinear distortion, resonators, superconducting devices.

I. Introduction

Nonlinearities in HTS materials cause degradation in device perfomance such as generation of intermodulation products and reduction of quality factors in resonators at high power levels. Several authors have been studying these effects [1]-[3] and theoretical work has been developed to quantify them in transmission lines with intrinsic HTS nonlinearities [4]. This work may be extended in two aspects: on one hand, it is necessary to accommodate nonlinear effects other than the ones intrinsic to the HTS; on the other, a practical way has to be found to model an overall device that includes several nonlinear HTS lines.

We have addressed both aspects in this paper. We present an algorithm to model devices with transmission lines containing distributed nonlinearities in the inductance and resistance per unit length. Almost any type of nonlinearities can be treated by this algorithm, as long as they can be expressed as a current-dependent inductance and/or resistance per unit length. Although HTS materials are known to produce these types of nonlinearities in transmission lines [4], we do not try to relate the HTS physics to the electrical parameters of a nonlinear transmission line. Rather, we discuss ways on how to extract these parameters from experimental measurements. We think this is a practical and realistic approach, since HTS nonlinearities are known to be strongly dependent on the fabrication process, and may even change from sample to sample.

The algorithm that we present also allows an efficient way to simulate devices (like filters and multiplexers) containing several nonlinear HTS lines. This is done with a netlist-based circuit simulator which can combine nonlinear transmission lines with standard circuit elements.

Manuscript received August 10, 2000.

Authors are with Universitat Politècnica de Catalunya (UPC), Campus Nord UPC D3, Barcelona 08034, Spain. (telephone 34-93-401 7229, email: joano@tsc.upc.es)

This work is supported by the Spanish Ministry of Education and Culture through project MAT-0984-C03-03 and scholarship AP99-78085980 for J. Mateu.

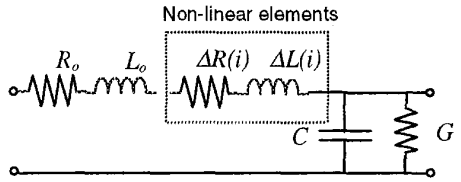

Fig. 1. Equivalent circuit of an elemental cell of a nonlinear transmission line

II. The MHB Algorithm

Our algorithm models nonlinear transmission lines (in the form of microstrip, stripline or coplanar waveguide) as a cascade of identical cells like the one in Fig. 1. To model the nonlinear effects of the HTS, the resistance and inductance in each elemental cell are assumed to be dependent on the total current [4].

If a microwave HTS device (such as a filter) can be modeled as different interconnected transmission lines, its equivalent circuit can be formed by including all the elemental cells from the lines, and the circuit elements used to interconnect the lines. This equivalent circuit will have a linear part characterized by an impedance matrix $\mathbf{Z}(\omega)$, which will be loaded with N nonlinear one-ports plus one excitation port (Fig. 2).

The voltages and currents through the N+1 ports must satisfy the matrix equation imposed by the linear network

$$\mathbf{V}=\mathbf{Z}(\omega)\,\mathbf{I}\ . \tag{1}$$

Also, the voltage across each nonlinear one-port v_{nl} is caused by the current crossing it, and must be calculated in time domain using:

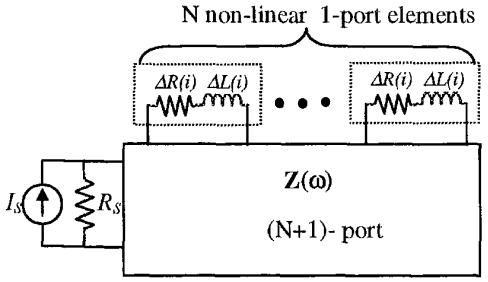

Fig. 2. Equivalent circuit of a device containing nonlinear HTS transmission lines.

$$v_{nl} = \Delta R(i) i + \frac{d}{dt}(\Delta\phi(i)), \tag{2}$$

where the magnetic flux $\Delta\phi(i)$ is related to the nonlinear inductance: $\Delta\phi(i)=\Delta L(i)\, i$.

To analyze the equivalent circuit of Fig. 2, the algorithm begins assuming zero initial conditions for all components of **V**, except that corresponding to the source port. Equation (1) is then used to obtain the vector of currents **I**. These currents, in time domain, are applied in (2) to find a first estimate of the voltages across the N non linear one-ports (v_{nl}).

The right solutions (voltages and currents) must satisfy (1) and (2) simultaneously and they are found by iterating the preceding process following a standard Harmonic Balance algorithm [5]. Note that the nonlinearities in (2) may cause frequency components not present in the excitation signal. Therefore, (1) must be evaluated for all possible frequency components: those of the excitation signals, and those of the spurious that they may produce.

A more detailed mathematical description of the application of the Harmonic Balance algorithm to nonlinear HTS transmission lines can be found in [6].

Note that this algorithm does not depend on a specific definition of $\Delta R(i)$ and $\Delta L(i)$. In the software developed, these can be easily changed by the user, or even adjusted automatically to match simulations with measurement results.

Our software finds $\mathbf{Z}(\omega)$ automatically for the whole equivalent circuit of Fig.2 (including all the cells of the nonlinear transmission lines) from a netlist supplied by the user. This netlist does not detail all the elemental cells in each line, instead it includes a description of each transmission line as a single element in the circuit.

We refer to this algorithm as Multiport Harmonic Balance (MHB) to distinguish it from the standard one, which is normally applied to lumped element circuits.

III. MHB CROSS-CHECK

To check the accuracy of MHB, the intermodulation behaviour of a HTS half-wave resonator has been compared against theoretical predictions. Several restricting assumptions are made: no dielectric losses, and a square-law dependence of $\Delta R(i)$ and $\Delta L(i)$ on the current i ($\Delta R(i)= \Delta R_2\, i^2$; $\Delta L(i)= \Delta L_2\, i^2$). Under these assumptions we have derived a closed form equation for the peak current of a third order intermodulation product:

$$\left|I_{2\omega_1-\omega_2}\right| = \frac{3|I_{\omega 1}|^2 |I_{\omega 2}| Q_L}{16} \left| \frac{3\Delta R_2}{Q_0 R_0} + j\frac{3\Delta L_2}{L_0} \right| \tag{3}$$

where $|I_{\omega 1}|$, $|I_{\omega 2}|$ are the peak values of the fundamental signals, and R_0, L_0 are the low field distributed parameters of the line. The derivation of (3) is done in a similar way as that outlined in [4]. This equation coincides with that described in [4], except for a factor 3 in the imaginary part due to the definition of the nonlinear magnetic flux in (2). We have used (3) to check our simulations with the values that can be inferred from [4]: $\Delta R_2=0$, $\Delta L_2 = 2.72\text{x}10^{-12}$ $H/(m\ A^2)$. Note from (3) that the amplitude of the intermodulation products would be the same for any pair of ΔR_2, ΔL_2 for which the term $\left|(\Delta R_2/Q_0 R_0) + j(\Delta L_2/L_0)\right|$ is constant.

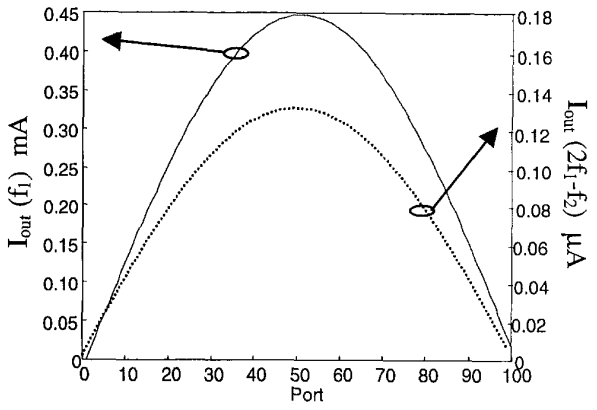

Fig. 3. Current distribution of fundamental and third order intermoluation currents along a half wave line resonator calculated by MHB.

Fig. 3 shows the standing wave pattern in the resonator for the fundamental and third order intermodulation currents. The half-wave resonator was divided into 100 unit cells (Fig.1), and the total simulation time was less than 3 s running on a Pentium III at 550 MHz.

A close agreement (within 0.2%) between (3) and the simulation was found for the peak current of the third order intermodulation product $I_{2\omega 1-\omega 2}$.

IV. AVOIDING AMBIGUITY IN THE DETERMINATION OF THE NONLINEAR PARAMETERS

If the intrinsic effects of the HTS were the only ones intervening in the nonlinear behaviour of a HTS line, only nonlinearities in the inductance per unit length would have to be considered [4]. However, if other extrinsic causes exist, the nonlineal resistance could contribute significantly to this behaviour [2], [7]. Therefore, the determination of $\Delta R(i)$ and $\Delta L(i)$ can be ambiguous if both elements have similar contributions to the experimental observables being considered. Fig. 4 shows an example of this. This figure shows the power of the fundamental signal and the intermodulation products as a function of the source power. It has been obtained by simulation assuming $\Delta R(i)= \Delta R_2\, i^2$ and $\Delta L(i)= \Delta L_2\, i^2$ and using two different pairs of values of ΔR_2, ΔL_2 ($\Delta R_2=0$, $\Delta L_2 = 2.72\text{x}10^{-12}$ $H/(m\ A^2)$; and $\Delta R_2 = 0.085$ $\Omega/(m\ A^2)$, $\Delta L_2 = 0$). The first pair of values is that used in Fig. 3. Note that for source powers below −10dBm both sets of data give almost identical results, and the determination of ΔR_2, ΔL_2 based solely on the power of the fundamental and intermodulation signals (as in Fig. 4) would be ambiguous.

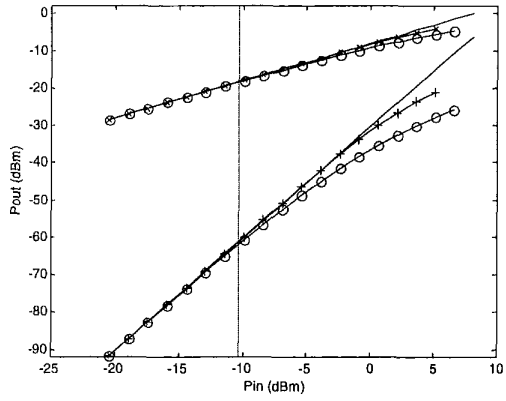

Fig. 4. Simulated output vs. input power for the fundamental and third order intermodulation signals in a two-port resonator. Lines with open circles correspond to data obtained with $\Delta L_2=0$; lines with crosses correspond to $\Delta R_2=0$. Solid lines are asymptotes for the small-signal behaviour, with slopes of 1:1 and 3:1. Coupling coefficients are 0.25 at both ports of the resonator.

Figs. 5 and 6 show other data that complements that in Fig. 4 and may help break this ambiguity. Fig. 5 shows the frequency response of the fundamental signal for the first pair of values ($\Delta R_2 = 0$). Fig. 6 is equivalent to Fig. 5, but has been obtained with the second pair of values ($\Delta L_2 = 0$). The change in resonant frequency and unloaded quality factor in these two figures is summarized in Table I. It is clear from these data that an unambiguous determination of ΔR_2, ΔL_2 can be made if the power levels are sufficiently high to cause an observable effect on the frequency response of the resonator. This determination can be made with MHB by jointly fitting measured data equivalent to Fig. 4 and the frequency response of the resonator (equivalent to Fig. 5 and 6).

V. Fitting Experimental Data

Our software has been used to fit experimental data mostly obtained by other groups. Our goal is to illustrate the capability of our software to determine $\Delta R(i)$ and $\Delta L(i)$. We do not claim avoid ambiguities in this determination, since we only have access to intermodulation data equivalent to that in Fig. 4, whereas a full set of data like the one described

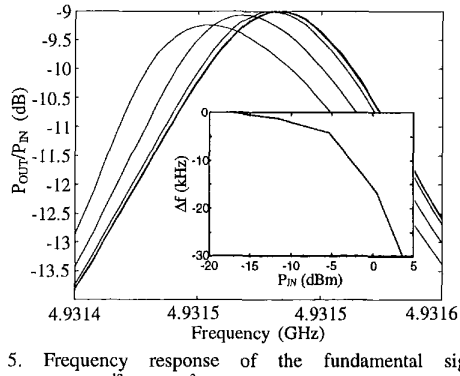

Fig. 5. Frequency response of the fundamental signal for $\Delta R_2=0$, $\Delta L_2=2.72\text{x}10^{-12}$ $H/(m\ A^2)$. Inset shows the change of the resonant frequency vs. source power. Simulations correspond to source power values of -17.45, -11.43, -5.41, 0.61 and 3.62 dBm

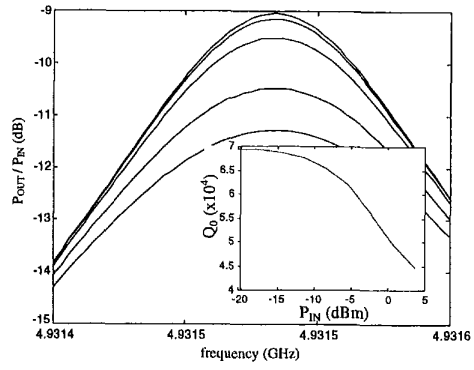

Fig. 6. Frequency response of the fundamental signal for ΔR_2 =0.085 $\Omega/(m\ A^2)$, ΔL_2 =0). Inset shows the reduction of the Q_0 vs. source power. Simulations correspond to the source power values of Fig. 5.

in the previous section (equivalent to Fig. 4 and Fig. 5 or 6) would be necessary to resolve the ambiguity. Nevertheless, we have been able to reproduce data fittings made in other works for simple resonators [8], and fit the behavior of multi-pole filters.

A. Hairpin resonator

The nonlinear performance of hairpin microstrip resonators is analyzed and measured in [8]. This reference claims that $\Delta R(i)\approx 0$ and attributes all nonlinear behavior to $\Delta L(i)$. Furthermore, $\Delta L(i)$ is found to be strongly dependent on the resonant modes, since magnetic field configurations vary significantly from even to odd modes. As detailed in [9], we have successfully fitted experimental data in [8]. In particular, for the second resonant mode we could reproduce the behavior of $\Delta L(i)$, which follows a square-law with i at low power levels, and is proportional to $|i|$ at high power levels.

B. Forward coupled filters

We have also fitted the intermodulation performance of two different forward-coupled microstrip filters assuming that the effects of $\Delta L(i)$ dominate over those of $\Delta R(i)$. In both cases, we have first found the linear elements of the equivalent circuit by fitting the small-signal scattering parameters. Then, $\Delta L(i)$ of the HTS microstrip lines has been adjusted to fit the power of the fundamental and intermodulation signals at the output.

Fig. 7 shows the results for a seven pole filter. We fitted the power of the fundamental signal and the intermodulation products for a source power above 0 dBm by making $\Delta L(i)$ proportional to $|i|$. The measured intermodulation power

TABLE I
Variation of Unloaded Quality Factor and Resonant Frequency

P_{IN} (dBm)	ΔQ ($\Delta L_2=0$)	ΔQ ($\Delta R_2=0$)	Δf_0 ($\Delta L_2=0$)	Δf_0 ($\Delta R_2=0$)
-20 to -10	2.6%	0.6%	≈ 0	1.2 KHz
-10 to 3	33.7%	9%	≈ 0	28.4KHz

Summary of changes of unloaded quality factor and resonant frequency in Figs. 5 and 6.

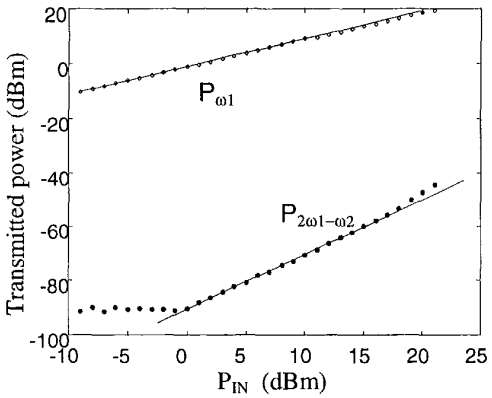

Fig. 7. Fundamental and third order intermodulation transmitted power vs. input power. These simulated data (lines) reproduce the measurements (dots).

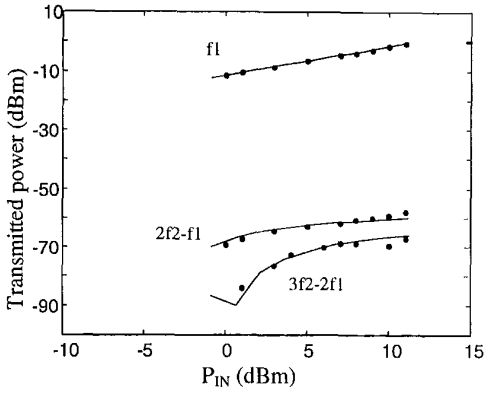

Fig. 9. Fundamental and third order intermodulation transmitted power vs. input power. These simulated data (lines) reproduce the measuremets (dots).

shows a plateau below 0dBm which may not be due to the superconductor.

Fig. 8 shows the spatial distribution of currents in the filter at both the fundamental and intermodulation frequencies. Each lobe in the figure represents one resonant line, and the rightmost and leftmost sections of the graph show the current distributions in the input and output lines. Our software can generate this type of graph at any pair of frequencies.

Fig. 9 shows a similar case for a nine pole filter that we measured. The measured data showed unusual features, like the slope of the intermodulation power, which was much lower than in the previous case. We had to fit the data with an exponential dependence of $\Delta L(i)$ with i^2, $\Delta L(i) = Ai^2 \exp(-Bi^2)$. With this dependence we could simultaneously fit the third and fifth order intermodulation products.

VI. Conclusions

The Harmonic Balance algorithm can be applied to simulate the distributed nonlinearities of HTS transmission lines. The algorithm can also be used to extract the nonlinear properties of the HTS lines by fitting measurements to simulated data. This fitting can be ambiguous if only the transmitted power of fundamental and spurious signals is considered.

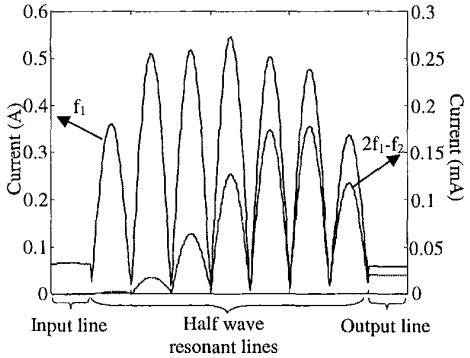

Fig. 8. Spatial distribution (current vs. distance) of currents in a 7 pole forward-coupled filter [10] at f_1 and $2f_1$-f_2. The half wave line resonators are placed parallel to each other. Each lobe represents the spatial current distribution in a line resonator.

Acknowledgements

The authors acknowledge the Microwave Superconductivity Group of University of Naples for the data on the seven pole forward-coupled filter, and Richard Taylor and Else Shepherd from Mosaic Information Technology, for the nine-pole forward-coupled filter. Salvador Talisa is also acknowledges for helpful comments and suggestions.

References

[1] D. E. Oates, A.C. Anderson, D.M. Sheen and S.M.Ali, "Stripline resonator measurements of Zs versus H_{rf} in Y Ba Cu O thin films", *IEEE Trans. on Microwave Theory and Tech.*, vol. 39, no. 9 pp. 1522-1529, Sept. 1991.

[2] O. G. Vendik, I. B. Vendik, T. B. Samoilova, "Nonlinearity of superconducting transmission line and microstrip resonator", *IEEE Trans on Microwave Theory and Tech.*, vol. 45, no. 2, pp. 173-178, Feb. 1997.

[3] S.Kolesov, H. Chaloupka, A. Baumfalk and T. Kaiser, "Planar HTS tructures for high power applications in communications systems," *J. Superc.*, vol. 10, no. 3, pp. 179-187, 1997.

[4] T. Dham and D.J. Scalapino, "Theory of intermodulation in superconducting microstrip resonator", *J. Appliel Physic*, vol. 81, no. 4, pp. 2002-2009, 1997.

[5] S. A. Maas, *Nonlinear Microwave Circuits* , Artech House, 1988.

[6] C. Collado, J. Mateu, J.M. O'Callaghan, "Computer simulation of the non-linear response of superconducting devices using the Multiport Harmonic Balance algorithm", *Inst. Of Phys. Conf. Ser. No.* 167 pp. 411-414, 2000.

[7] J.H. Oates, R.T. Shin, D.E. Oates, M.J Tsuk, P.P. Nguyen, "A nonlinear transmission line model for superconducting stripline resonators", *IEEE Trans. On Appl. Superc.*, vol. 3, no. 1, pp. 17-22, 1993.

[8] B. A. Willemsen, T. Dahm and D. J. Scalapino, "Microwave intermodulation in thin film high-Tc superconducting microstrip hairpin resonators: Experiment and theory", *Appl. Phys. Lett.* vol. 71, no. 29, pp. 3898-3900, 1997.

[9] C. Collado, J. Mateu, J. Parron, J. Pons, J.M. O'Callaghan, J.M. Rius, "Harmonic balance algorithms for the nonlinear simulation of HTS devices", submitted to *J. of Supercond.*

[10] G. Pica, A. Andreone, A. Cassinese, M. Iavarone, P. Orgiani, F. Palomba, M. Salluzzo, R. Vaglio, R. Monaco, R. Russo. "A Superconducting Based Front End Receiver for GSM1800 Base Stations". *Applied Superconductivity Conference 2000.* Virginia Beach, Virginia, Sept. 2000.